Direct epitaxial growth of subsurface Co nanoclusters

T. Siahaan, O. Kurnosikov, H. J. M. Swagten, and B. Koopmans
Department of Applied Physics, Eindhoven University of Technology, 5600 MB Eindhoven, Netherlands
(Received 1 May 2014; revised manuscript received 24 September 2014; published 15 October 2014)

A new subsurface growth mode in the Co-Cu system is reported. This mode provides a direct subsurface growth of Co nanoclusters by depositing Co atoms on the Cu(001) surface in a single stage. The resulting subsurface Co nanoclusters are located 2 monolayers (ML) deep below the atomically flat surface of Cu(001). Although these hidden nanoclusters cannot be directly accessed by a scanning tunneling microscopy/spectroscopy (STM/STS) probe, their shape could be deduced using STM/STS via a careful analysis of the local deformation of the Cu(001) surface as well as local variations of surface electron density induced by the subsurface clusters. A strongly asymmetric shape of the nanoclusters is deduced: they are typically 5-10 nm in lateral size but only 2 to 3 ML in thickness. The thickness of the nanoclusters does not evolve significantly under a heat treatment. A simple model is implemented to describe the growth kinetics. The results in this study reveal that intense processes of diffusion, nucleation, and growth take place in a region 1 nm deep, thus defining the near-surface region.

DOI: 10.1103/PhysRevB.90.165419 PACS number(s): 68.35.Dv, 68.37.Ef, 81.07.−b, 81.15.Hi

I. INTRODUCTION

Metal-on-metal heteroepitaxial growth usually aims at the formation of thin and flat films, although a further downsizing in the lateral dimensions can also be realized. This downsizing leads to a formation of nanoislands, nanoclusters, or other nanostructures *on* top of a surface [1–10]. A direct formation of *subsurface* nanostructures is generally not achieved via single-stage epitaxial growth modes. To obtain subsurface structures, a combination of deposition methods such as codeposition, capping on-the-surface structures, and alternating deposition is usually needed [11,12]. In this paper the direct formation of subsurface Co nanoclusters in Cu(001) using a single epitaxial growth step is reported. Such a single-step deposition process has not been realized before and could be interesting for future applications, particularly when it would lead to, e.g., enhanced magnetic anisotropies observed in other studies on buried nanostructures [11,13].

Previous studies revealed that Co growth on Cu(001) at room temperature results in Co structures on top of the surface [14,14–26]. The solubility of Co in bulk Cu is very low [27,28]. Considering this, incorporation of Co very deep into the Cu substrate, which should precede the growth of the nanoclusters, would be very unlikely. However, there is much experimental evidence of incorporation of single Co atoms in the first layer of Cu(001) after deposition even at room temperature [15–19]. The intermixing of Co and Cu can involve even a couple of near-surface layers at elevated temperatures. This indicates that the solubility of Co in surface and near-surface systems cannot be judged by a simple analysis of the bulk phase diagrams. Taking into account physical processes that are governed by stress generation or vacancy concentration, one can expect a gradual change from the surface towards the bulk physical properties within a few atomic layers. This opens the possibility for Co accumulation in the near-surface region. Furthermore, thermodynamic considerations of surface and interface energies of the Co-Cu system indicate that the formation of subsurface clusters is favorable. The free surface energy of Co ($\gamma_{\mathrm{Co}} = 2.55\ \mathrm{J\,m^{-2}}$) is higher than the sum of the free surface energy of Cu ($\gamma_{\mathrm{Cu}} = 1.85\ \mathrm{J\,m^{-2}}$) and the Co-Cu interface energy ($\gamma_{\mathrm{Co\text{-}Cu}} = 0.25\ \mathrm{J\,m^{-2}}$) [29,30]. As a consequence, Co structures, such as films or islands, would prefer to be surrounded by Cu rather than to be located on the free surface [20,31–33]. For a comparison with another system, the growth of subsurface islands upon Cu deposition on Pb(111) was reported [34]. This is attributed to a similar relation between surface and interface energies for Cu and Pb. Therefore, one can expect that the formation of subsurface Co clusters in Cu(001) will take place if proper growth parameters are chosen.

The formation of subsurface clusters should involve Co diffusion in the region below the Cu(001) surface. Since this process is thermally activated, temperature becomes a crucial parameter. From studies on thin-film growth of Co on Cu(001), it is obvious that room temperature is not high enough to activate this diffusion into the region below the surface. To activate subsurface diffusion, deposition should be performed at a significantly higher substrate temperature. Previous studies on Co growth on Cu(001) at elevated temperatures indeed indicated the possibility to get subsurface Co. Studies with scanning tunneling microscopy, Auger electron spectroscopy, and low-energy electron diffraction reported by Ramsperger *et al.* revealed that Co goes below the surface upon deposition on Cu(001) at 540 K [23]. However, no detailed description of the structure created was reported. In a different but related system, Zimmermann *et al.* reported the phenomenon of burrowing of Co *particles* upon their direct deposition on Cu(001) at 600 K [35]. These studies coherently reported that Co does not tend to stay on the surface or in the first layer of the substrate upon deposition at elevated temperatures.

Considering the suggestions and the reports discussed above, we found a regime of subsurface epitaxial growth. This regime was successfully obtained by elevating the substrate temperature above the value commonly used for the growth of a Co thin film on Cu(001). Co deposition on such a hot Cu surface was found to lead to the direct growth of subsurface Co nanoclusters. As shown in this paper, a temperature of around 650 K provides an efficient incorporation of Co atoms in a region 1 nm deep below the surface where the subsurface growth

takes place. At this temperature further Co incorporation into deeper regions of Cu is still hampered. A detailed study of this subsurface structure is performed using scanning tunneling microscopy/spectroscopy (STM/STS). Although STM/STS is known as a surface analysis technique, the local surface deformation and local variation of surface electron density that are induced by the subsurface nanoclusters enable utilization of STM/STS for characterization of these hidden nano-objects. Insight on the growth kinetics of the clusters is obtained by varying the nominal coverage of deposition and applying heat treatments.

This paper is organized as follows. The next section gives a general explanation of the experiment. In Sec. III the structures obtained after Co deposition on hot Cu(001) are described. Sections IV and V describe the characterization of the subsurface nanoclusters, addressing their shape and depth, respectively. Section VI describes the growth kinetics of the nanoclusters. Section VII summarizes and concludes this study.

II. EXPERIMENTS

Subsurface Co nanoclusters were formed after Co deposition on a hot (650 K) single-crystal Cu(001) substrate. Prior to deposition, the substrate was cleaned in vacuum using a sputter-anneal procedure. Co was deposited with different nominal coverages, ranging from 0.1 to 1.43 monolayers (ML), using the *e*-beam evaporation technique from a calibrated Co source (deposition rate = 0.22 ML/min) at a base pressure below 5×10^{-10} mbar. All sample preparation and characterization were done *in situ* in an ultrahigh-vacuum (UHV) system (Omicron).

The samples were characterized by STM/STS at 78 K using electrochemically etched W tips. The base pressure during measurements was below 10^{-10} mbar. STM measurements provide topographic maps. Analysis of specific features in the images gives the values of the lateral size as well as the thickness.

STS provides surface differential conductance maps at the scanned surfaces as well as the tunneling conductance spectra $dI/dV(V)$ and the tunneling current spectra $I(V)$ at selected locations. A lock-in technique was used with a modulation of 50 mV peak to peak superimposed on the bias voltage. The surface differential conductance mapping was performed together with the STM topographic imaging at constant bias voltages while the feedback loop was closed. The $dI/dV(V)$ spectra were measured with the feedback loop open while varying the bias voltage. These conductance spectra were measured together with the $I(V)$ spectra.

Characterization of samples with different nominal Co coverages provides information about the kinetics of the growth. More insight on the kinetics of the growth is gained from an extra heat treatment. In this treatment, the samples containing Co clusters were heated up to the deposition temperature and kept at that temperature for various times followed by STM/STS measurements.

III. STRUCTURES AFTER COBALT DEPOSITION ON A HOT SUBSTRATE

After a 650 K deposition of 0.85 ML of Co, STM images reveal an atomically flat Cu surface, as shown by

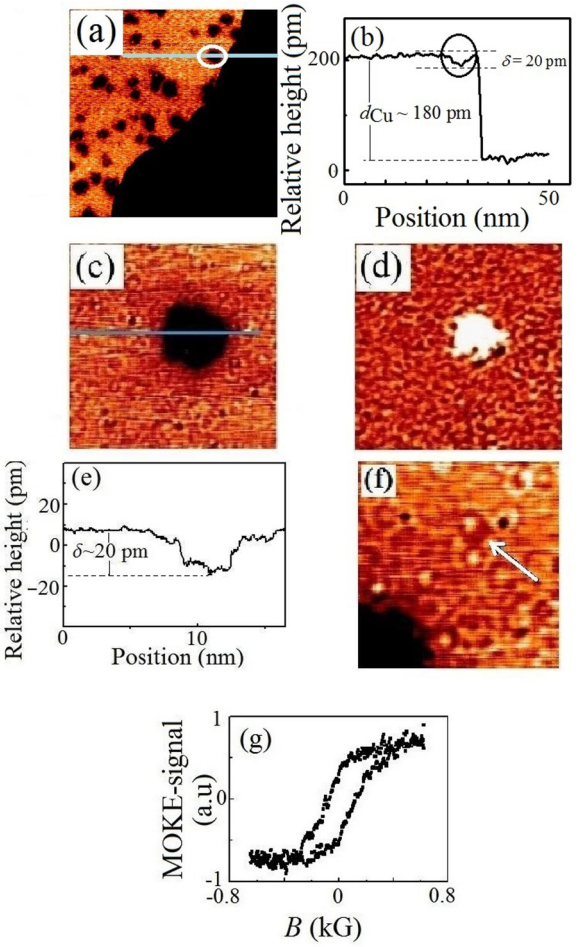

FIG. 1. (Color online) (a) Morphology of the Cu(001) surface (70×70 nm^2) after 0.85-ML Co deposition at 650 K. The tunneling set point is (0.4 V, 1 nA). The bright and dark areas are two neighboring atomically flat terraces. Surface depressions are visible as spots on the terraces. (b) The surface cross section along the line shown in (a). The ellipse indicates the same surface depression indicated by the white ellipse in (a). (c) A typical STM image (18×18 nm^2) of a surface with a surface depression. The tunneling set point is (0.2 V, 1 nA). (d) The surface differential conductance map corresponding to the area shown in (c) at the same tunneling set point. (e) The surface cross section along the line shown in (c). (f) STM image of an area (11.25×11.25 nm^2) with the ringlike ripples in between the depressions. The arrow shows one of the ringlike ripples. The tunneling set point is (−0.2 V, 1 nA). (g) A result of an *ex situ* room temperature magneto-optic Kerr effect measurement.

Fig. 1(a), instead of islands on top of the surface, which are usually obtained after a room-temperature deposition. A similar observation was reported by Ramsperger *et al.* after a deposition at 540 K [23]. In Fig. 1(a) one can see a surface with two atomically flat terraces that differ in height by ∼180 pm [Fig. 1(b)], corresponding to the interlayer distance of Cu(001) d_{Cu}. However, shallow depressions on the surface with typical lateral sizes of 5–10 nm and depths δ of around 20 pm were observed on these flat terraces [Fig. 1(b)]. More detailed STM and STS images [Figs. 1(c) and 1(d)] reveal that the depressions correlate to a local enhancement of surface

differential conductance. This is observed as spots with bright contrasts in the surface differential conductance maps exactly at the positions of the depressions for bias voltages ranging from 0.1 to 0.6 V. Surface profiles across the depressions [a typical one is shown in Fig. 1(e)] reveal that δ ranges between 16 and 22 pm, which corresponds to 9%–12% of d_{Cu}. Since these depressions and the corresponding enhanced conductance are not observed in STM and STS images of clean Cu(001) without Co deposition, they should be attributed to the presence of Co.

Although the variation of the local density of the electronic state may contribute to the surface profiling by STM, the observed depressions are real. In Sec. IV B we show that the electronic effects on our sample can only slightly reduce the apparent depth of the depressions determined from their cross sections.

In addition to the depressions and the enhanced conductance, Figs. 1(c) and 1(d) show ripples elsewhere. These ripples originate from single Co atoms dissolved within a few subsurface layers of the Cu substrate. More detailed analysis of the ripples, given by Fig. 1(e), shows that they are formed by superposition of ringlike structures with a diameter ranging from 0.5 up to 2 nm. Exactly the same ringlike structures were reported by Weismann *et al.* as the result of a perturbation of the surface electron density due to the presence of single Co atoms below the (001) and (111) surfaces of Cu [36]. The diameter of the single rings is determined by the depth of the single scattering center represented by a Co atom in the Cu matrix. Thus, part of the deposited Co is also present as single atoms in the near-surface region. This additional feature will be discussed later.

Besides being partially dissolved near the surface, Co also forms nanoclusters as deduced from additional *ex situ* magneto-optic Kerr effect measurements at room temperature. Figure 1(g) shows one of the magnetic hysteresis loops obtained from the measurements on the samples in this study. This ferromagnetic signal can only be explained by ferromagnetic objects such as Co nanoclusters. Single Co atoms that are dissolved in the Cu matrix would only provide a paramagnetic signal [37]. Thus, the hysteresis loops confirm that the observed surface depressions should be associated with Co nanoclusters.

The nanoclusters can be located either *in the first layer* of the substrate or *below* the surface as no islands on the surface are shown by STM images [Figs. 1(a) and 1(c)]. Both configurations would cause the appearance of depressions due to the lattice mismatch between Co ($a_{Co}^{fcc} = 3.54$ Å) and Cu ($a_{Cu} = 3.61$ Å). A theoretical work by Stepanyuk *et al.* shows that the latter case is favorable since the configuration of buried Co clusters has a lower energy [33]. Nevertheless, the first case should also be analyzed.

By comparing the $dI/dV(V)$ and $I(V)$ spectra measured on the depressions with the ones measured on a reference sample, it is concluded that the clusters are embedded below the Cu surface. Such a sample was fabricated by an additional deposition of Co on a cold (~250 K) sample that already contained the embedded Co nanoclusters. Thus, the reference sample contained both the embedded clusters and 1- and 2-ML-thick free Co islands on the surface, as sketched in the bottom left corner of Fig. 2.

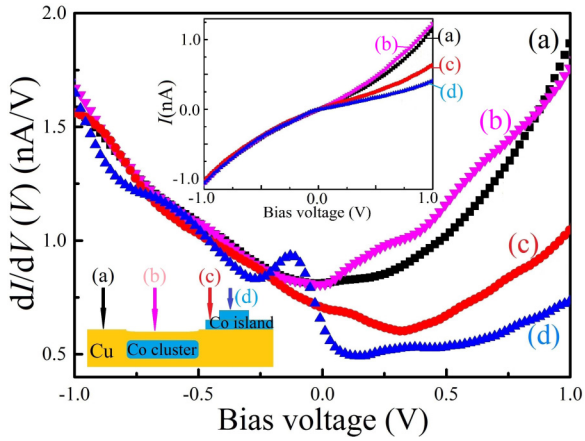

FIG. 2. (Color online) The surface differential conductance spectra $dI/dV(V)$ measured with a tunneling set point of (−1 V, 1 nA). The spectra are measured on (a) the clean Cu surface (black), (b) depressions (magenta), and Co islands that are (c) 1 ML (red) and (d) 2 ML (blue) thick. The inset shows the corresponding $I(V)$ spectra. The schematic of the structure of the reference sample is given in the bottom left corner.

The $dI/dV(V)$ and $I(V)$ spectra measured on the reference sample are shown in Fig. 2. The spectrum from a clean Cu surface [labeled (a)] is almost featureless, as expected for a Cu(001) surface [38]. The spectrum measured on the depressions [labeled (b)] is very similar to the spectrum from a clean Cu surface, with only a minor enhancement in the positive bias voltage region. In contrast, the spectra measured on Co surfaces, represented by 1-ML-thick [spectrum (c)] and 2-ML-thick [spectrum (d)] Co islands, deviate strongly from the spectrum measured on Cu [spectrum (a)], particularly with much lower values in the positive bias voltage region. If the nanoclusters were embedded in the first layer, exposing a free Co surface at the depressions, one would expect a strong deviation of the spectrum measured on the depressions from the ones measured on Cu, similar to what is shown by spectra (c) and (d) in Fig. 2. In fact, there is no such strong deviation between spectra (b) and (a) from Cu. Therefore, spectrum (b) is due to tunneling between the tip and a Cu surface. This implies that the Co nanoclusters must be located underneath the Cu surface. The subsurface nanoclusters just affect the electron density at the Cu surface above each of them, causing a small deviation of spectrum (b) from spectrum (a). This deviation is considered in Sec. V to deduce the depth of the nanoclusters.

IV. SHAPE OF THE NANOCLUSTERS

A. Lateral size

Based on the observed line profiles across the surface depressions, these depressions can be described by Fig. 3. From this the lateral size of the nanoclusters can be deduced. Such an analysis of STM images results in a typical value of 5–10 nm. The amount of deposited Co is found to influence mainly the density of the depressions and hardly affects the lateral size.

Considering this deduced lateral size together with the surface coverage of the depressions and the nominal amount

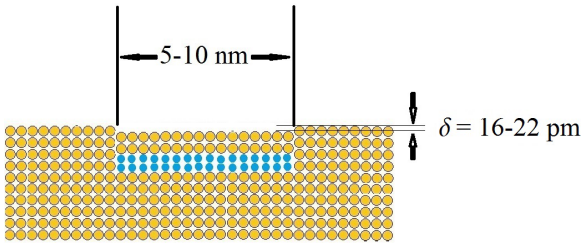

FIG. 3. (Color online) A schematic side view of a Co cluster embedded below a Cu substrate, resulting in a depression at the surface with a depth δ. The blue circles represent Co atoms, while the orange ones represent Cu atoms.

of deposited Co provides an estimation of the typical shape of the nanoclusters. A more or less three-dimensional (3D) symmetric shape would be expected for an isotropic 3D growth as in the case of Ar nanoclusters formed deep below the Cu(001) [39,40] and Cu(110) [41–43] surfaces. However, a simple analysis reveals that this is not the case. The nanoclusters should be very thin. The *upper limit* of possible thicknesses of the nanoclusters can be determined simply by dividing the total volume of Co deposited on the covered area by the depressions. For example, upon a deposition of 1 ML of Co, the depressions cover ∼15% of the surface. With such an analysis one finds that, in principle, the nanoclusters cannot be thicker than ∼1.3 nm (7 ML). This value is much smaller than the average lateral size (7.7 nm) of the nanoclusters in that sample. Their actual shape is determined from a detailed analysis of the thickness of the nanoclusters as presented below.

B. Thickness estimation

A more precise thickness estimation can be done by analyzing the depth δ of the depressions which originate from the lattice mismatch between Co and Cu. Assuming that they possess a face-centered-tetragonal structure like Co films grown epitaxially on Cu(001) do [20,44–47], their interatomic layer spacing in the third dimension should be the same as it is in epitaxial Co films on Cu(001). The average value of the depth of depressions ranges from 16 to 22 pm (9% to 12% of d_{Cu}). Considering an overall interatomic layer distance in the Co clusters, reported to be 4% smaller than $d_{\mathrm{Cu(001)}}$ for epitaxially grown Co films on Cu(001) [45], the thicknesses of the clusters is estimated to be 3 or 4 ML. However, when dealing with ultrathin Co films, significant relaxations at the Co-Cu interfaces as well as in the Cu and Co layers close to the interfaces should be considered [20,46,47]. Besides this relaxation, a slight difference in the electron density above the clusters can affect the real surface profiling obtained with the constant-current mode of the STM operation. Both the relaxation and electronic effects can lead to a miscalculation of the nanocluster thickness if only the simplest approach of a defined lattice mismatch is considered.

To estimate the uncertainty of the Co nanocluster thickness due to the electronic effects, we compared the apparent depth of the depressions measured at various bias voltages. The apparent depth difference does not exceed 6 pm. This experimental result is in good agreement with another comparison based on the free-electron tunneling model [48]. It limits the apparent depth difference to 8 pm considering the observed conductance curves. These numbers correspond to the uncertainty of the thickness of the Co nanoclusters being less than 1 ML. Taking into account these numbers and the fact that the depressions always show enhanced conductance [Fig. 1(d)], one can consider the actual Co nanoclusters to be slightly thicker, but not by as much as one extra atomic layer.

In contrast, when extra relaxations are taken into account, the nanoclusters are estimated to be thinner. Using interlayer distances between Co layers and the Co-Cu layers at the interface reported in an experimental study by Cerda *et al.* [46], the thickness of the clusters is estimated to be 2 or 3 ML, assuming that both interfaces in the clusters relax in a symmetric way. On the other hand, taking into account the relaxations calculated by Spišák and Hafner [47] leads to the conclusion of a maximum thickness of 3 ML. Furthermore, considering relaxations in the system of Cu-capped Co islands *on top* of a Cu(001) surface suggests even thinner nanoclusters that are 1 ML thick [20]. Nevertheless, one should notice that the latter structure is not stable [20].

Obviously, the lack of consistent data on the relaxation of Co layers as well as the possible influence of the electronic density of states above the clusters hinders an unambiguous determination of the thickness. Nevertheless, the analysis above indicates that a thickness in the range between 1 and 3 ML is the most likely. A more precise determination of the thickness using two other approaches based on the local variation of the surface electron density and the surface coverage of the depressions is discussed in Secs. V and VI, respectively. These two approaches are combined with an auxiliary analysis of the evolution of the depression depth. In that analysis, the relative change of the depth of the depressions as a function of the nominal coverage is considered. The consideration of this relative change instead of an absolute value makes the analysis more reliable. In this way the influence of relaxation and electronic effects on the final result is suppressed or negligible.

C. Stability of the shape

A thickness of 1, 2, or 3 ML for subsurface nanoclusters with a lateral size of 5–10 nm, meaning a very high aspect ratio ($\geqslant$10), could be considered to be surprising. Usually, one considers the minimization of the total interface energy to be the driving factor for the resulting shape. Since the clusters are embedded below the surface, implying the substrate already possesses bulk properties, they could be expected to have a 3D symmetric shape such as a Wulff-like construction (with consideration of the interface energy). However, the actual shape of the subsurface clusters deviates strongly from this expectation. This raises the question of whether these ultrathin clusters would remain very thin or undergo a 3D symmetrization under a heat treatment. The latter scenario should lead to a gradual increase of the cluster thickness upon annealing. This could be monitored by carefully measuring the depth evolution of the depressions because it is correlated with the change of thickness.

In the heat treatment, three parameters from the STM measurements were deduced: (i) the average depth, averaging

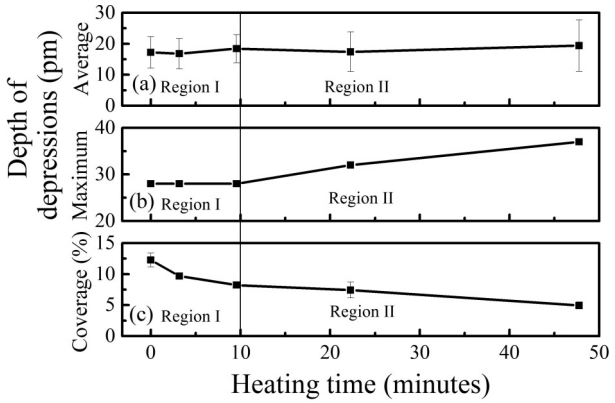

FIG. 4. Time dependence of the (a) average and (b) maximum depth of the depressions and (c) their surface coverage under a heat treatment at 650 K. The sample was fabricated by deposition of 0.7 ML of Co on a hot Cu(001) surface. The vertical line divides the plots into regions I and II, which correspond to treatment times less than and more than 10 min, respectively. The error bars in (a) and (c) show the standard deviations of the data distribution.

the depth over the entire depressed regions, (ii) the maximum depth, averaging the deepest point of each depression over the complete ensemble, and (iii) the surface coverage, normalizing the depressed area of the total scan area. We note that a difference between average and maximum depths is indicative of regions with different thickness within a single Co cluster.

The time dependences of the average and maximum depths of the depressions under the heat treatment at a deposition temperature of 650 K are shown in Figs. 4(a) and 4(b). Figure 4(a) shows a relatively constant average depth of depressions throughout the treatment. Region I in Fig. 4(b) shows no increase in the maximum depth (28 ± 1 pm) of the depressions after heating for less than 10 min (about 3 times the deposition time). On the other hand, Fig. 4(c) shows a continuous decrease of the lateral size of the clusters, which indicates a loss of Co from the clusters due to diffusion, which will be discussed further later. After a treatment for a longer time the maximum depth of the depression increases. Region II in Fig. 4(b) shows such an increase up to 32 ± 1 pm after a treatment for 22 min and up to 37 ± 2 pm after 48 min. The mentioned errors are the standard deviation of the mean, where the sampling number ranges from 28 to 50. As the depressions, which originate from the lattice mismatch between Co and Cu, become deeper by up to 9 ± 3 pm, it can be concluded that the clusters become thicker by only 1 ML. This shows that the thickness of the nanoclusters is only marginally affected and that the nanoclusters certainly do not evolve towards a 3D symmetric shape after the heat treatment at the deposition temperature.

The evolution of the shape of the nanoclusters towards a 3D symmetric shape probably takes a much longer time. To speed up the process, an additional treatment at 690 K was performed. However, after less than 2 hours, no strong increase in the average or maximum depth of the depressions was observed. Moreover, after more than 3 hours the topographic and surface differential conductance maps did no longer revealed any dips or contrasts. This was also the case after a treatment for another sample at a much higher temperature (800 K) for 5 min, indicating that the Co atoms from the clusters were totally dissolved into the substrate. Thus, in the near surface a heat treatment does not, in principle, lead to a 3D symmetrization of the clusters until the Co atoms are completely dissolved.

V. DEPTH OF THE LOCATION OF THE NANOCLUSTERS

The Co nanoclusters below a Cu(001) surface induce a deviation of the electron density at the surface above each cluster, as evidenced by Fig. 2 [compare spectra (a) and (b)]. Such a deviation observed at different depressions and for samples can be systematically analyzed using $[dI/dV(V)]/[I(V)/V]$ spectra with a normalization to the spectra from the clean Cu surface. In Fig. 5(a) the Cu-normalized $[dI/dV(V)]/[I(V)/V]$ spectra from different depressions and samples are shown by the colored spectra. Differences between various spectra can be attributed to individual parameters of the nanoclusters such as their size or shape. Despite these small differences, the spectra are generally of similar shape. The average of these spectra is shown by the black spectrum and will be used for further analysis.

The shape of these Cu-normalized $[dI/dV(V)]/[I(V)/V]$ spectra can be associated with the depth and thickness of the Co nanoclusters. This is because the deviation of the

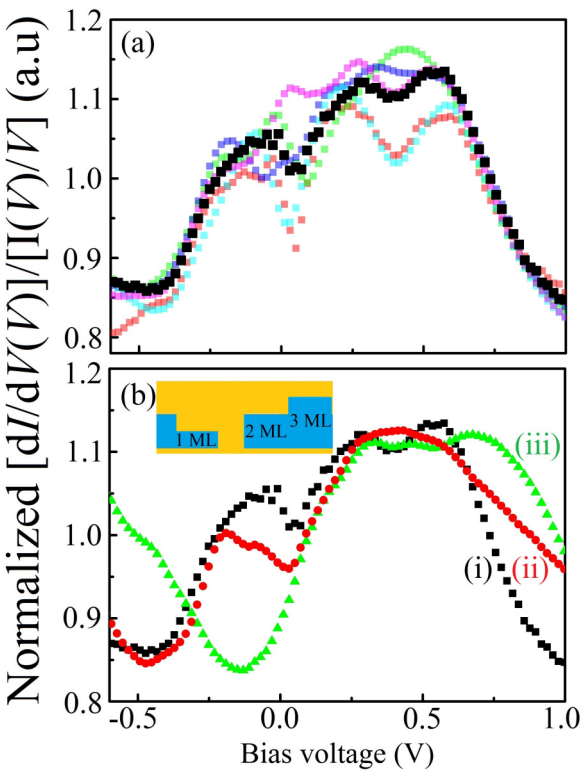

FIG. 5. (Color online) (a) Cu-Normalized $[dI/dV(V)]/[I(V)/V]$ spectra from various depressions obtained after 0.6- and 0.8- ML Co depositions. The averaged spectrum is shown by black squares. (b) Spectrum (i) is the averaged spectrum from the depressions, the same as in (a). Spectra (ii) and (iii) are two selected spectra from the calibration sample. The schematic picture of the calibration sample is in the top left corner. All spectra were measured with a tunneling set point of (−1 V, 1 nA).

electron density at the surface should be dependent on how deep the nanoclusters are located as well as how thick they are. Therefore, the depth and thickness of the nanoclusters can be determined experimentally by comparing the actual spectra with the ones measured on a calibration sample containing a known Cu/Co/Cu(001) structure. The calibration sample was fabricated separately by subsequent Co and Cu depositions by *e*-beam evaporation on a clean Cu(001) substrate. The resulting sample contained Co layers 1, 2, and 3 ML thick buried below an atomically flat Cu surface at a controllable depth while part of the surface was still a clean Cu surface, as shown by the inset in Fig. 5(b).

Figure 5(b) shows the averaged spectrum from the depressions [spectrum (i)], which is the same as that shown in Fig. 5(a), together with two selected examples of spectra [(ii) and (iii)] from the calibration sample. The shape of spectrum (ii) is very similar to that of spectrum (i) with minor deviations between −0.5 and 0.7 V. Spectrum (iii) deviates significantly from spectrum (i), revealing the absence of the peak around −0.1 V. Both spectra (ii) and (iii) are actually obtained from similar 2-ML-thick Co layers covered by Cu layers but with different thicknesses of copper. Spectrum (ii) is obtained with a 2-ML-thick Cu covering layer, while spectrum (iii) is obtained with a 3-ML-thick one. One can see that a difference of only 1 ML in the Cu layer thickness leads to a remarkable deviation from spectrum (i). No other combination of Co and Cu layers (not shown here) gives a similarity that is better than that of the combination of 2 ML of Cu and 2 ML of Co. Based on this analysis, it is concluded that the Co nanoclusters are located 2 ML below the surface, with their thickness being 2 ML.

VI. MODELING

A. Surface coverage versus nominal coverage plot

To get insight into the growth kinetics, an analysis of the surface coverage is done together with a modeling analysis. These also provide an alternative determination of the thickness of the clusters. This analysis considers the surface coverage of the dips Φ, presented as percentages, as a function of the nominal coverage θ. The function $\Phi(\theta)$ depends on and reflects the thickness of the clusters. As the deposition time in our study was always less than 10 min, a two-dimensional (2D) growth mode is expected, as shown by Figs. 4(a) and 4(b) and the previous discussion. Therefore, one might expect that this corresponds to a constant thickness of n ML of Co nanoclusters, where n can be 1, 2, or 3. With the assumption that the dissolution of Co in Cu and the diffusion of Co to the bulk region can be neglected, this mode should lead to a linear relation:

$$\Phi = \frac{100\%}{n\ \mathrm{ML}}\theta. \qquad (1)$$

The straight lines, which are expected from Eq. (1), deviate remarkably from the experimental $\Phi(\theta)$ plot, as shown in Fig. 6(a). Overall, the $\Phi(\theta)$ plot reveals two surprising features. First, cluster formation was not observed up to 0.2-ML Co deposition, while it was observed after a Co deposition of 0.35 ML. This means there is an onset θ_s (0.2 ML $< \theta_s <$ 0.35 ML) for cluster formation [see the gray area in Fig. 6(a)]. Second, the plot does not show a linear relation between Φ and θ as described by Eq. (1).

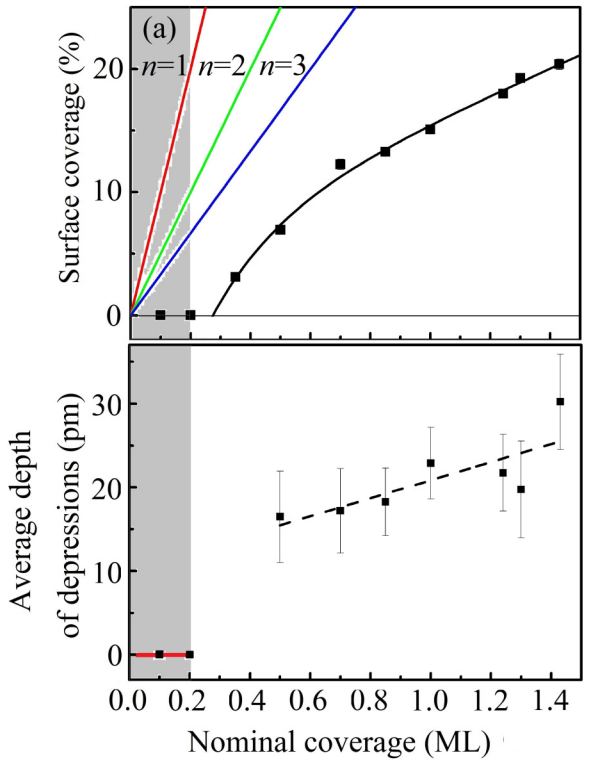

FIG. 6. (Color online) (a) The surface coverage and (b) average depth of the depressions vs the nominal coverages θ. Straight lines in (a) show the expected surface-nominal coverage dependencies based on the simplified assumptions given by Eq. (1) for clusters thicknesses of 1 (red), 2 (green), and 3 (blue) ML. The solid squares represent the experimental results. The solid fitted curve in (a) is obtained from the model equation (2) with $n = 2$. The dashed line in (b) is a guide to the eyes showing the data tendency. The gray area indicates the experimental regime where no surface depressions were found. The error bars show the standard deviation of the data distribution.

Additionally, Fig. 6(b) shows the average depth of the surface depressions versus θ. After the onset of $\theta \leqslant 0.2$ ML, where zero depth is reported, this plot shows a quick jump to the value of 17 pm, followed by an increase of the depression depth from 17 to 25 pm within 0.5 ML $\leqslant \theta \leqslant$ 1.43 ML. The depth difference of about 8 pm corresponds to an increase in the thickness of the Co cluster by approximately one single atomic layer. This means that the actual increase of the thickness following the growth is limited, excluding a 3D type of growth related to the actual cluster sizes.

The onset of cluster formation is similar to what was observed previously for the growth of surface Co structures on Cu(001) at room temperature. In that case, Co surface islands are not formed after a Co deposition for $\theta \leqslant 0.25$ ML [15,16,26]. Although the onset that appears in the room-temperature surface growth has been explained well [16,26], one should note that the explanation for the reported onset of the subsurface growth in the present paper is still not clear.

The onset indicates the need to have Co accumulation up to a certain concentration in the near surface prior to cluster formation. This accumulation is not expected within the actual temperature range. Although a weak diffusion of Co into the bulk of Cu can occur at this deposition temperature, it should only be a minor effect due to its low rate. With an activation energy of 2.22 eV [49], Co diffusion in bulk Cu becomes significant only at a temperature $\geqslant$800 K. However, the appearance of ringlike ripples in the topographic maps [see Fig. 1(e)] evidences the presence of single Co atoms near the Cu(001) surface, as mentioned earlier. Thus, it is concluded that subsurface Co diffusion in the substrate during the deposition should occur in the near-surface region, while the bulk diffusion in deeper regions is still limited. As a consequence, Co accumulates near the surface.

The curved shape of the $\Phi(\theta)$ plot can originate from a process of Co segregation from the clusters as well as the formation of thicker clusters during growth. Co segregation takes place as Co atoms diffuse away from the clusters and then go farther into the deeper region via a weak bulk diffusion that is assumed to take place. This segregation process is confirmed by the heat treatment. Figure 4(c) shows a decrease in the surface coverage of the depressions, which indicates a decrease in the lateral size of the clusters. This can be due to cluster segregation as well as the formation of thicker clusters. Since the formation of thicker clusters is not noteworthy in region I in Fig. 4, as concluded previously, the decrease in the surface coverage shown in that region should be mainly attributed to Co segregation.

Besides Co segregation, formation of thicker clusters may also contribute to a curving of the $\Phi(\theta)$ plot. In this case, the clusters nucleate with the initial thickness n ML. Under higher nominal coverages the clusters develop laterally while each cluster can also partially reach the thickness of $n+1$ ML. This is consistent with Fig. 6(b). Therefore, the growth of the Co clusters can still be considered in the framework of the 2D type of growth of a complex system characterized by two thicknesses.

B. Growth description

Based on the previous discussion, a simple phenomenological model is proposed to describe the growth of Co nanoclusters. This model mainly takes into account Co subsurface diffusion near a Cu(001) surface.

The growth starts with Co diffusion and accumulation in the region several atomic layers below the Cu(001) surface [Figs. 7(a) and 7(b)]. After the required Co concentration to initiate cluster formation is reached, further deposition of Co leads to an agglomeration of Co atoms. This leads to a formation of initial clusters with a stable thickness of n ML [Fig. 7(c)], where n is initially assumed to be 1, 2, or 3, as deduced in Sec. IV B.

The growth of the initial clusters in lateral dimensions takes place as the deposition continues. Part of the deposited Co, denoted by α, participates in this growth, while the remainder diffuses into the deeper region of the substrate via weak bulk diffusion. The growth of lateral dimensions is described by an increase of the partial surface coverage Φ_n at a rate of $R\alpha \times 100\%/(n\ \mathrm{ML})$, where R is the deposition rate.

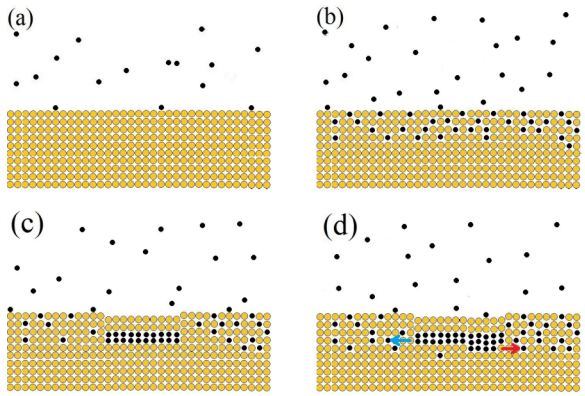

FIG. 7. (Color online) A schematic illustration of the main processes considered in the model described by Eq. (2). The black circles represent the Co atoms, while the orange ones represent the Cu atoms. (a) Start of Co deposition on a hot Cu(001) substrate. (b) Incorporation and accumulation of Co in the near-surface region. (c) Formation of an initially n-ML-thick Co cluster. (d) Further growth of the initial clusters, accompanied by the formation of the next layer as well as Co segregation from the initial cluster (blue arrow) and the thicker cluster (red arrow).

During the growth of the initial clusters, Co atoms in these n-ML-thick clusters can form thicker clusters with a thickness of $n+1$ ML, and they can also segregate to leave the clusters. The formation of thicker clusters increases the partial coverage Φ_{n+1} at a rate proportional to Φ_n. The segregation takes place at a rate proportional to the area of the Co-Cu interface, which is thus proportional to Φ_n and Φ_{n+1}.

This growth model is described by the following set of differential equations:

$$\frac{d\Phi_n}{dt} = \frac{R\alpha \times 100\%}{n\ \mathrm{ML}} - s_n\Phi_n - (n+1)f_n\Phi_n + s_{n+1}\Phi_{n+1},$$
$$\frac{d\Phi_{n+1}}{dt} = nf_n\Phi_n - s_{n+1}\Phi_{n+1}, \qquad (2)$$

for $t \geqslant t_s$. Here, t_s is the required deposition time to reach the onset θ_s, and $\Phi = \Phi_n + \Phi_{n+1}$. The parameters s_n and s_{n+1} are fitting parameters related to the segregation of the n- and $(n+1)$-ML-thick clusters, respectively, and f_n is the fitting parameter related to the formation of $n+1$ ML thick clusters. In the present form, Eq. (2) can be solved analytically.

The analytical solutions for various n of Eq. (2) (see the Appendix) are fitted to the experimental data. Figure 6(a) shows the best fitting, which is obtained for $n=2$. The fitting for $n=3$ leads to unphysical values of the parameters, while the fitting for $n=1$ is possible, although it is less satisfactory than that for $n=2$. This fitting for $n=2$ suggests that the first 2-ML-thick clusters nucleate after an onset deposition of 0.26 ML of Co. During lateral growth, the transformation of the 2-ML cluster to the 3-ML clusters takes place. This results in a final configuration of clusters with combined partial thicknesses of 2 and 3 ML.

The thickness suggested by this model is in good agreement with the estimated thickness deduced in Sec. IV B. It is realized that the exact thickness of the nanoclusters still cannot be determined from solely this simple model. To determine the exact thickness of the clusters a more advanced model which

takes various atomic processes into account in more detail is certainly required. Nevertheless, taking into account the analysis in Sec. V, it is likely that the nanoclusters initially grow with an initial thickness of 2 ML.

VII. SUMMARY AND CONCLUSIONS

A subsurface growth mode in the epitaxial system of Co and Cu is obtained by a Co deposition on a hot (650 K) Cu(001) substrate. This mode results in Co nanoclusters located below an atomically flat Cu surface. The shape and the depth of the nanoclusters are deduced experimentally by a careful analysis of data acquired using STM/STS. The growth kinetics is also studied by implementing a simple phenomenological model that describes the growth of the nanoclusters. Combining the analysis of both the experimental and modeling results, it is revealed that the nanoclusters have lateral sizes of 5–10 nm and thicknesses of 2 to 3 ML. Their location is also revealed to be 2 ML deep below the surface.

The deduced parameters suggest that the processes of Co diffusion and cluster nucleation which govern the growth of the subsurface Co nanoclusters take place in a region below the surface that is up to 5 ML (∼1 nm) deep. Since such processes are different from the ones in the bulk, this implies that the region that can be attributed to the near surface is ∼1 nm deep.

In this study the capability of STM/STS to locally detect features on the surface which are induced by the subsurface structures has been used to characterize the subsurface Co nanoclusters. This demonstrates the possibility of extending the use of this surface-sensitive technique to not only surface but also subsurface studies.

ACKNOWLEDGMENTS

The authors are grateful to J. T. Kohlhepp and W. J. M. de Jonge for discussions and suggestions that improved the presentation of this study. This study is part of the research program of the Dutch Foundation for Fundamental Research on Matter (FOM), which is part of the Netherlands Organisation for Scientific Research (NWO).

APPENDIX

Depending on parameters $a_{\pm}$, where

$$a_{\pm} = \frac{-[s_n + (n+1)f_n + s_{n+1}] \pm \sqrt{[s_n + (n+1)f_n + s_{n+1}]^2 - 4s_{n+1}(s_n + nf_n)}}{2}, \tag{A1}$$

the solution of Eq. (2) can be given by different expressions. For the case of $a_+ \neq a_-$, the solution is given by

$$\begin{aligned} \Phi_n &= \frac{R\alpha \times 100\%}{n \text{ ML}} \left[\frac{s_{n+1}}{a_+ a_-} + \frac{1 + s_{n+1}/a_+}{a_+ - a_-} e^{a_+(t-t_s)} + \frac{1 - s_{n+1}/a_-}{a_+ - a_-} e^{a_-(t-t_s)} \right], \\ \Phi_{n+1} &= \frac{f_n R\alpha \times 100\%}{\text{ML}} \left\{ \frac{1}{a_+ a_-} + \frac{1}{a_+ - a_-} [e^{a_+(t-t_s)} - e^{a_-(t-t_s)}] \right\}. \end{aligned} \tag{A2}$$

For the case of $a_+ = a_- = a$, the solution is given by

$$\begin{aligned} \Phi_n &= \frac{R\alpha \times 100\%}{n \text{ ML}} \left\{ t e^{a(t-t_s)} + \frac{s_{n+1}}{a^2} [1 + at e^{a(t-t_s)}] \right\}, \\ \Phi_{n+1} &= \frac{f_n R\alpha \times 100\%/\text{ML}}{a^2} [1 + at e^{a(t-t_s)}]. \end{aligned} \tag{A3}$$

[1] D. D. Chambliss, R. J. Wilson, and S. Chiang, Phys. Rev. Lett. **66**, 1721 (1991).
[2] R. Q. Hwang, J. Schröder, C. Günther, and R. J. Behm, Phys. Rev. Lett. **67**, 3279 (1991).
[3] R. Q. Hwang, C. Günther, J. Schröder, S. Günther, E. Kopatzki, and R. J. Behm, J. Vac. Sci. Technol. A **10**, 1970 (1992).
[4] C. Yu, D. Li, J. Pearson, and S. D. Bader, Appl. Phys. Lett. **78**, 1228 (2001).
[5] B. Müller, L. Nedelmann, B. Fischer, H. Brune, J. V. Barth, and K. Kern, Phys. Rev. Lett. **80**, 2642 (1998).
[6] M. C. Bartelt and J. W. Evans, Surf. Sci. **314**, L829 (1994).
[7] H. J. Elmers, J. Hauschild, H. Höche, U. Gradmann, H. Bethge, D. Heuer, and U. Köhler, Phys. Rev. Lett. **73**, 898 (1994).
[8] J. Shen, R. Skomski, M. Klaua, H. Jenniches, S. S. Manoharan, and J. Kirschner, Phys. Rev. B **56**, 2340 (1997).
[9] B. Voigtländer, G. Meyer, and N. M. Amer, Phys. Rev. B. **44**, 10354 (1991).
[10] P. Carrozzo, F. Tumino, M. Passoni, C. E. Bottani, C. S. Casari, and A. L. Bassi, Surf. Sci. **619**, 77 (2014).
[11] T. Koide, H. Miyauchi, J. Okamoto, T. Shidara, A. Fujimori, H. Fukutani, K. Amemiya, H. Takeshita, S. Yuasa, T. Katayama, and Y. Suzuki, Phys. Rev. Lett. **87**, 257201 (2001).
[12] O. Fruchart, M. Klaua, J. Barthel, and J. Kirschner, Phys. Rev. Lett. **83**, 2769 (1999).
[13] F. Luis, F. Bartolomé, F. Petroff, J. Bartolomé, L. M. García, C. Deranlot, H. Jaffrès, M. J. Martínez, P. Bencok, F. Wilhelm, A. Rogalev, and N. B. Brookes, Europhys. Lett. **76**, 142 (2006).
[14] A. K. Schmid and J. Kirschner, Ultramicroscopy **42–44**, 483 (1992).

[15] J. Fassbender, R. Allenspach, and U. Dürig, Surf. Sci. **383**, L742 (1997).
[16] F. Nouvertné, U. May, M. Bamming, A. Rampe, U. Korte, G. Güntherodt, R. Pentcheva, and M. Scheffler, Phys. Rev. B. **60**, 14382 (1999).
[17] S.-K. Kim, J.-S. Kim, J. Y. Han, J. M. Seo, C. K. Lee, and S. C. Hong, Surf. Sci. **453**, 47 (2000).
[18] F. Nouvertné, U. May, A. Rampe, M. Gruyters, U. Korte, R. Berndt, and G. Güntherodt, Surf. Sci. **436**, L653 (1999).
[19] T. Bernhard, R. Pfandzelter, M. Gruyters, and H. Winter, Surf. Sci. **575**, 154 (2005).
[20] R. Pentcheva and M. Scheffler, Phys. Rev. B. **61**, 2211 (2000).
[21] W. A. Jesser and J. W. Matthews, Philos. Mag. **17**, 461 (1968).
[22] M. T. Kief and W. F. Egelhoff, Jr., Phys. Rev. B. **47**, 10785 (1993).
[23] U. Ramsperger, A. Vaterlaus, P. Pfäffli, U. Maier, and D. Pescia, Phys. Rev B. **53**, 8001 (1996).
[24] N. Levanov, V. S. Stepanyuk, W. Hergert, O. S. Trushin, and K. Kokko, Surf. Sci. **400**, 54 (1998).
[25] R. A. Miron and K. A. Fichthorn, Phys. Rev. B. **72**, 035415 (2005).
[26] R. Pentcheva and M. Scheffler, Phys. Rev. B. **65**, 155418 (2002).
[27] M. Hansen and K. Anderko, *Constitution of Binary Alloys* (McGraw-Hill, New York, 1958).
[28] T. Nishizawa and K. Ishida, J. Phase Equilibria **5**, 161 (1984).
[29] J. Gerkema and A. R. Miedema, Surf. Sci. **124**, 351 (1983).
[30] A. R. Miedema and F. J. A. Den Broeder, Z. Metallkd. **70**, 14 (1979).
[31] H. Li and B. P. Toner, Surf. Sci. **237**, 141 (1990).
[32] A. K. Schmid, D. Atlan, H. Itoh, B. Heinrich, T. Ichinokawa, and J. Kirschner, Phys. Rev. B. **48**, 2855 (1993).
[33] V. S. Stepanyuk, D. V. Tsivline, D. I. Bazhanov, W. Hergert, and A. A. Katsnelson, Phys. Rev. B. **63**, 235406 (2001).
[34] C. Nagl, E. Platzgummer, M. Schmid, P. Varga, S. Speller, and W. Heiland, Phys. Rev. Lett. **75**, 2976 (1995).
[35] C. G. Zimmermann, M. Yeadon, K. Nordlund, J. M. Gibson, R. S. Averback, U. Herr, and K. Samwer, Phys. Rev. Lett. **83**, 1163 (1999).
[36] A. Weismann, M. Wenderoth, S. Lounis, P. Zahn, N. Quaas, R. G. Ulbrich, P. H. Dederichs, and S. Blügel, Science **323**, 1190 (2009).
[37] S. Chikazumi, *Physics of Ferromagnetism* (Oxford University Press, New York, 1997).
[38] P. Kloth, M. Wenderoth, P. Willke, H. Prüser, and R. G. Ulbrich, Phys. Rev. B. **89**, 125412 (2014).
[39] O. Kurnosikov, O. A. O. Adam, H. J. M. Swagten, W. J. M. de Jonge, and B. Koopmans, Phys. Rev. B. **77**, 125429 (2008).
[40] O. Kurnosikov, J. H. Nietsch, M. Sicot, H. J. M. Swagten, and B. Koopmans, Phys. Rev. Lett. **102**, 066101 (2009).
[41] O. Kurnosikov, H. J. M. Swagten, and B. Koopmans, Phys. Rev. Lett. **106**, 196803 (2011).
[42] O. Kurnosikov, D. V. Kulikov, V. S. Kharlamov, H. J. M. Swagten, and Y. V. Trushin, Phys. Rev. B. **84**, 054109 (2011).
[43] D. V. Kulikov, O. Kurnosikov, V. S. Kharlamov, and Y. V. Trushin, Appl. Surf. Sci. **267**, 128 (2013).
[44] A. Clarke, G. Jennings, R. F. Willis, P. J. Rous, and J. B. Pendry, Surf. Sci. **187**, 327 (1987).
[45] O. Heckman, H. Magnan, P. le Fevre, D. Chandesris, and J. J. Rehr, Surf. Sci. **312**, 62 (1994).
[46] J. R. Cerdá, P. L. de Andres, A. Cebollada, R. Miranda, E. Navas, P. Schuster, C. M. Schneider, and J. Kirschner, J. Phys. Condens. Matter. **5**, 2055 (1993).
[47] D. Spišák and J. Hafner, Phys. Rev. B. **62**, 9575 (2000).
[48] C. J. Chen, *Introduction to Scanning Tunneling Microscopy* (Oxford University Press, New York, 2008).
[49] R. Döhl, M.-P. Macht, and V. Naundorf, Phys. Status Solidi A **86**, 603 (1984).